Engineering Innovations
ISSN: 2813-1002, Vol. 19, pp 115-124
doi:10.4028/p-GzP1hK

Submitted: 2025-01-03
Revised: 2026-02-03
Accepted: 2026-02-28
Online: 2026-06-11

Effect of Surface Roughness on the Friction Moment in a Ball Bearing

Harsh Kumar[1,a*] and Mayank Tiwari[2,b]

[1]Mechanical Engineering Department, Indian Institute of Technology Patna, Patna 801106, India

[2]Mechanical Engineering Department, Indian Institute of Technology Palakkad, Kanjikode 678623, India

[a]harsh_2021me08@iitp.ac.in, [b]mayankt@iitp.ac.in

Keywords: Ball bearings, Lubrication, Rough surface, Friction torque

Abstract. Ball bearings are crucial components in various machinery and mechanical systems, finding applications across numerous industries such as automotive, aerospace, manufacturing, robotics, and household appliances. Minimizing friction and wear in the bearings is essential to enhance the efficiency, reliability, and lifespan of equipment. Friction moments in ball bearings occur due to rolling-sliding motion at the ball-race contact and sliding between the ball and cage. The magnitude of these friction moments depends on factors such as surface topography, load, and speed. Understanding how surface topography influences the friction moments in these bearings is crucial. This paper investigates the effect of surface roughness on the friction moment between the ball and race contact, as well as between the ball and cage contact. An analytical model is employed to estimate the friction torque within ball bearings, considering the total friction torque generated at the contact points between the balls and the race, as well as at the ball-cage interface. A mixed elastohydrodynamic lubrication model is used to estimate the friction coefficient at these contact points.

Introduction

Bearings are commonly used in automobiles, industry and energy. Single-row ball bearings are especially favoured for their simple design, ability to run at high speeds, and low maintenance costs. However, heat resulting from the power loss due to internal friction in these bearings can affect running torque, which in turn reduces the performance and reliability of systems [1]. Load, speed, and surface roughness are some parameters that influence friction torque, making it crucial to understand and predict it accurately to improve system efficiency and optimize bearing performance.

In ball bearings, there are contacts at the ball-race interface and ball-cage interface. Due to this, there is a generation of friction moments. At the ball-race contact, rotational resistance is primarily caused by microslip, which results due to conformity or spin [2]. Additionally, there is a hysteresis-induced resistance torque in ball bearings [3]. However, in the event of ball-cage contact, the skidding between the balls and cage creates a friction moment. [4].

Several research works are done in the past to understand the influence of surface topography and texture on friction moment for such contacts. Under lubricated conditions, surface roughness has been shown to significantly affect the interaction between balls and screws, as it plays a key role in forming and stabilizing the lubricating film, which reduces direct asperity contact [5, 6]. This can also be observed in the case of cylindrical roller bearings [7]. Gouda et al. [8] studied the effects of micro-texture placement on the inner race on radial ball bearing tribodynamic performance. Han et al. [9] explored the impact of groove factor and surface roughness on tribological behavior and instability in dry contact.

In ball bearings, the impact of surface roughness on friction torque has not been thoroughly investigated. An analytical model for calculating the frictional moment generated due to contacts between the ball and cage and the ball and race in a low-speed, lubricated ball bearing is presented in this study. The model estimates the friction coefficient at the contact locations using a mixed elastohydrodynamic lubrication (EHL) technique. Ball-race and ball-cage friction moments are examined in relation to surface roughness and speed. This analysis also looks at how these parameters affect the contact force between the ball and the cage.

Theoretical Model

An analytical framework of the schematic shown in Fig. 1 for calculating the friction moment in a lubricated ball bearing is explained in this section. The model is composed of three elements: ball-race interaction, ball-cage interaction, and a mixed EHL model. The friction torque at the ball-race contact (T_{rb}) is analyzed under static conditions, whereas the friction moment at the ball-cage contact (T_{cb}) is assessed dynamically. A mixed EHL model is employed to calculate the friction coefficient at these contact points.

Total frictional moment (T_{bb}) in ball bearings is the combined result of the frictional torques generated at the ball-race contact and the ball-cage contact [10], expressed in Eq. 1:

$$T_{bb} = T_{rb} + T_{cb} \tag{1}$$

This study makes some assumptions to streamline the modeling process and remove less important aspects. First, friction moments due to dust covers and seals are excluded in this model since it is made for open bearings. Secondly, it ignores frictional moments due to lubricant drag losses, churning, and splashing. Lastly, it is assumed that the contact patch at the site of contact follows the Hertzian contact principle and that the bodies undergo local elastic deformation.

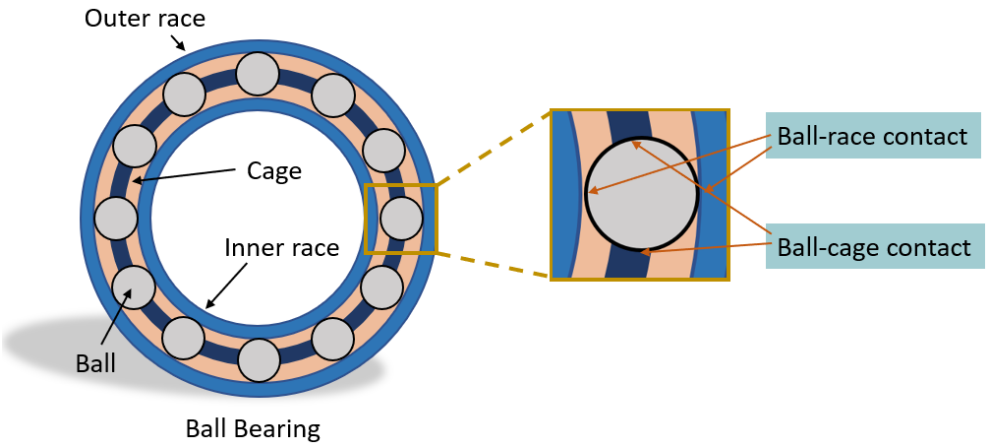

Fig. 1 A schematic representing different contacts in a ball bearing

Ball-Race Friction Torque Model. Microslip at ball-race contacts, as explained by Mindlin et al. [2], generates motion resistance in ball bearings. This leads to a rolling moment (M_r) and spin moment (M_z), as shown in Fig. 2, calculated using Eq. 2–7 based on the spin-to-roll ratio (ϵ). Pure rolling line positions (γ_1 and γ_2) depend on ϵ. Friction coefficient μ_{rb} is determined using a mixed EHL model.

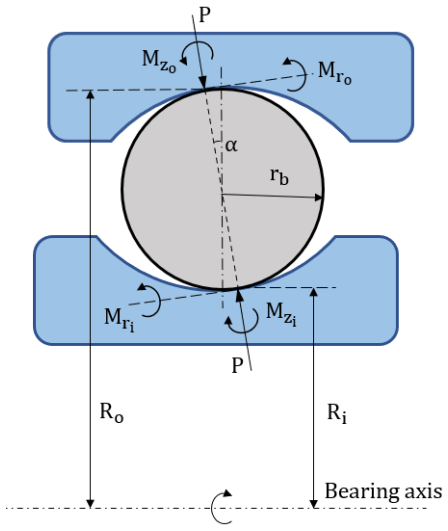

Fig. 2 Cross-sectional view of ball-race contact

If $\epsilon = 0$,

$$M_z = \frac{\mu_{rb} F_n b^2}{4 r_b} \tag{2}$$

$$M_r = 0 \tag{3}$$

If $0 < \epsilon < 0.5$,

$$M_z = \frac{3\mu_{rb} F_n b}{4}\left(\gamma_1^2\left(1 - \frac{\gamma_1^2}{2}\right) - \gamma_2^2\left(1 - \frac{\gamma_2^2}{2}\right)\right) \tag{4}$$

$$M_r = \frac{\mu_{rb} F_n b^2}{4 r_b}\left(\frac{2}{5} + \gamma_1^3\left(1 - \frac{3\gamma_1^2}{5}\right) - \gamma_2^3\left(1 - \frac{3\gamma_2^2}{5}\right)\right) \tag{5}$$

If $\epsilon \geq 0.5$,

$$M_z = 0 \tag{6}$$

$$M_r = 0.375 \mu_{rb} F_n b \tag{7}$$

A rolling element moving along a raceway under compressive force experiences stress relief at the back while the front portion of the contact patch contracts in the rolling direction. A moment called the hysteresis rolling moment is produced by such repetitive stress underneath the rolling track. Rolling moment due to hysteresis (M_h) is calculated using Eq. 8 (Ref. [11], p. 285).

$$M_h = \frac{3\alpha' F_n a}{16} \tag{8}$$

As a result, the total friction moment at the ball-race contact (T_{rb}) is the sum of all the moments produced at this contact.

$$T_{rb} = T_{conformity} + T_{spin} + T_{hysteresis} \tag{9}$$

where

$$T_{spin} = Z \times (M_z) \sin \alpha \tag{10}$$

$$T_{conformity} = Z \times \frac{(M_{ri} R_o + M_{ro} R_i)}{2 r_b} \tag{11}$$

$$T_{hysteresis} = Z \times \frac{(M_{hi} R_o + M_{ho} R_i)}{2 r_b} \tag{12}$$

Ball-Cage Friction Torque Model. This ball-cage friction torque model is based on Jiang et al.'s model [4]. Fig. 3 illustrates the various reference frames utilized in the model. Frame s is the stationary frame fixed to the bearing axis, frame c is the reference frame attached to the centre of the cage, frame b is connected to the centre of the ball, and frame p is associated with the centre of the pocket.

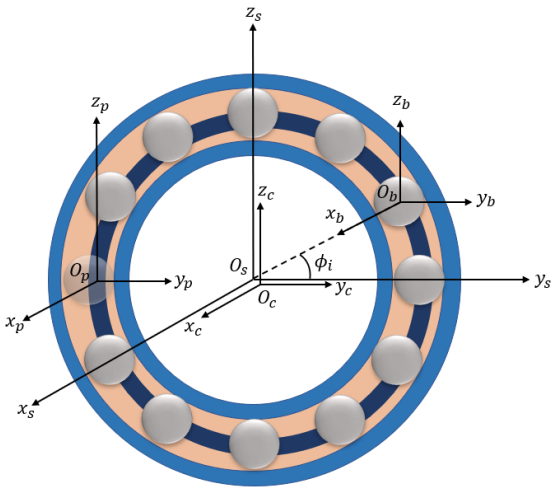

Fig. 3 Representation of different reference frames

There are three possible contact scenarios at the ball-cage contact: single-point contact, double-point contact, and no contact, as depicted in Fig. 4. If ε≥∇ and Δx≠0, there is a single-point contact, if ε≥∇ and Δx=0, there is a double-point contact, while no contact arises when ε<∇.

$$\varepsilon = \sqrt{\left(|\Delta x| + \left|\frac{D_p}{2} - k\right|\right)^2 + \Delta y^2 + \Delta z^2},\ \nabla = \frac{D_p}{2} - \frac{D_b}{2} \tag{13}$$

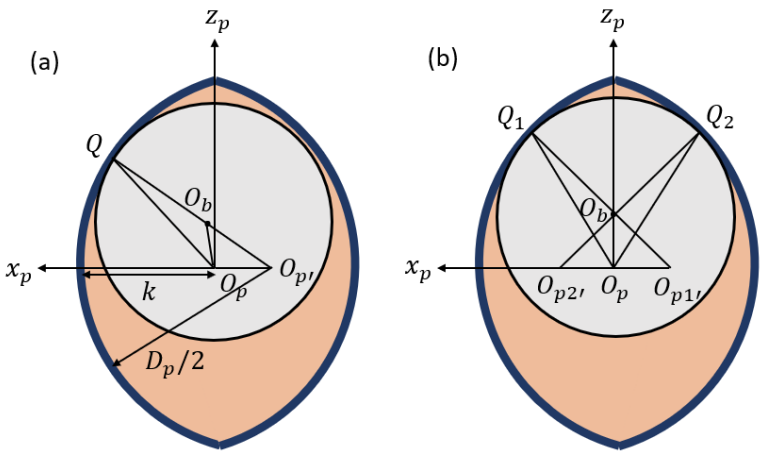

Fig. 4 (a) single point contact (b) double point contact

Assuming Hertzian contact, normal contact force (F^p_{pbN}) at ball-cage contact is determined from the contact deformation (δ_{pb}).

$$\left|F^p_{pbN}\right| = K_{pb}\delta^{\frac{3}{2}}_{pb} \tag{14}$$

$$F^p_{pbN} = \left|F^p_{pbN}\right| N^p_{pb} \tag{15}$$

where $\delta_{pb} = \varepsilon - \nabla$ and K_{pb} is the contact stiffness

Now, using the cage's tangential relative linear velocity and the ball-cage normal contact force, the tangential contact force (F^p_{pbT}) can be calculated. The mixed EHL model is used to determine the friction coefficient at the ball-cage contact (μ_{cb}).

$$F^p_{pbT} = -\mu_{cb}\left|F^p_{pbN}\right| \frac{\Delta v^p_{cbT}}{\left|\Delta v^p_{cbT}\right|} \tag{16}$$

Using Eq. 17, the ball-cage contact force is calculated.

$$F^p_{pb} = F^p_{pbN} + F^p_{pbT} \tag{17}$$

After calculating the ball-cage contact force, total force vector (F^c) and total moment vector (M^c) in frame c are obtained by using Eq. 18-19.

$$F^c = \sum_{i=1}^{z} T_{pc_i} F^p_{pb} \tag{18}$$

$$M^c = \sum_{i=1}^{z} T_{pc_i}\left(r^p_{cq} \times F^p_{pb}\right) \tag{19}$$

where $T_{pc_i} = {T_{cp_i}}^{-1}$

Mixed Elastohydrodynamic Lubrication Model. In the mixed elastohydrodynamic lubrication (EHL) model, the total load (F_T) is divided between the asperity load (F_a) and the load supported by the lubricant film (F_h) [12]. Both asperities and the lubricant film shear, creating frictional forces at

the contact surfaces. The asperity shear force is determined by adding the shear force from each asperity calculated by employing the asperity contact model by Zhao et al. [13]. Nijenbanning's numerical solution [14] for elliptical contact is employed to calculate the central film thickness. The shear stress is then calculated using the Eyring shear stress, and the shear force within the film is determined by multiplying the shear stress by the hydrodynamic area. The formula for determining the total frictional force produced in contacting surfaces is given by Eq. 21. The friction coefficient is then determined using Eq. 22.

$$F_t = F_a + F_h \tag{20}$$

$$F_f = F_{f,a} + F_{f,h} \tag{21}$$

$$\mu = \frac{F_f}{F_t} \tag{22}$$

Methodology

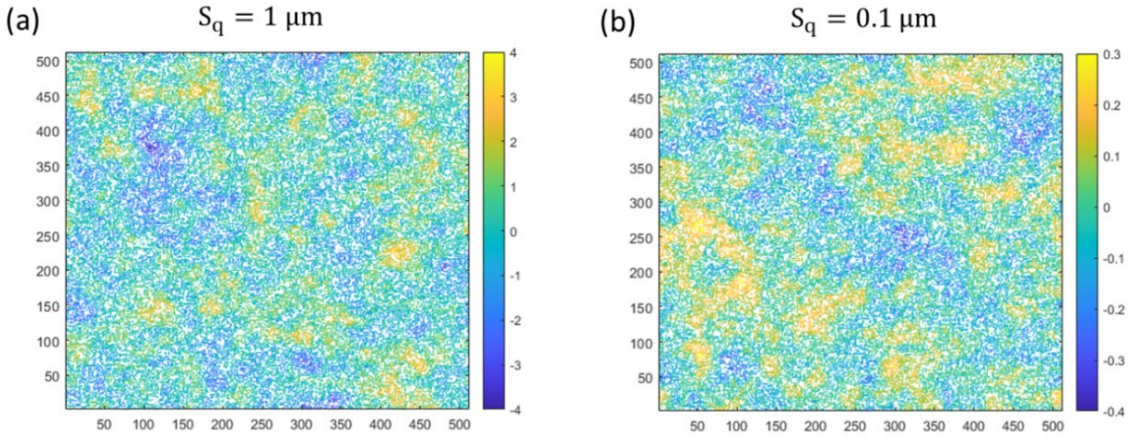

Fig. 5 Numerically generated rough surface of (a) Sq = 1 µm and (b) Sq = 0.1 µm

In this paper, the effect of surface roughness on friction torque is analyzed. For the analysis, a 6205 ball bearing is considered, with its design parameters provided in Table 1. Rough surfaces with RMS roughness values of Sq = 1 µm and Sq = 0.1 µm are numerically generated under the assumption of a Gaussian distribution. Fig. 5 illustrates the generated rough surface. The mixed EHL model uses these numerically produced surfaces as input to predict the friction coefficient. The analysis is conducted under a constant axial load of 1000 N, with the outer race fixed and the inner race rotating at speeds from 100 to 500 RPM in 100 RPM increments.

Table 1 Input parameters for the 6205 ball bearing.

Parameters	Value
Number of balls, **Z**	9
Mass of ball, $\mathbf{M_b}$	2.04 [gm]
Mass of cage, $\mathbf{m_c}$	6.58 [gm]
Contact angle, $\boldsymbol{\alpha}$	0.18 [rad]
Ball diameter, $\mathbf{D_b}$	7.94 [mm]
Mass of inner race	38.63 [gm]
Mass of outer race	54.21 [gm]
Radius of inner race	15.53 [mm]
Radius of outer race	23.48 [mm]
Groove radius of inner race	4.13 [mm]
Groove radius of outer race	4.21 [mm]
Pocket diameter	13.9 [mm]
Pocket depth	6.81 [mm]

Results and Discussion

This section examines a 6205 ball bearing's friction moment, highlighting the impact of speed and surface roughness. The impact of these variables on the estimated friction coefficient is also investigated in the study. In order to comprehend its contribution to ball-cage friction moment, the impact of surface roughness on the ball-cage contact force is also examined.

Variation of total friction moment. The variation of total friction moment (Nmm) with speed (RPM) for a 6205 ball bearing for two different surface roughness levels (Sq = 1 μm and Sq = 0.1 μm) is shown in Fig. 6. For both surface roughness, the data indicates that friction torque rises with rotational speed. Bearings with higher surface roughness (Sq = 1 μm) consistently demonstrate greater friction torque compared to those with smoother surfaces (Sq = 0.1 μm) across all speeds. The friction torque rises from 17.89 Nmm at 100 RPM to 25.09 Nmm at 500 RPM for the rougher surface (Sq = 1 μm). Conversely, the friction torque increases from 8.67 Nmm at 100 RPM to 12.90 Nmm at 500 RPM for the smoother surface (Sq = 0.1 μm). These results indicate that higher surface roughness significantly amplifies frictional losses, underscoring the importance of smoother surfaces in minimizing friction torque.

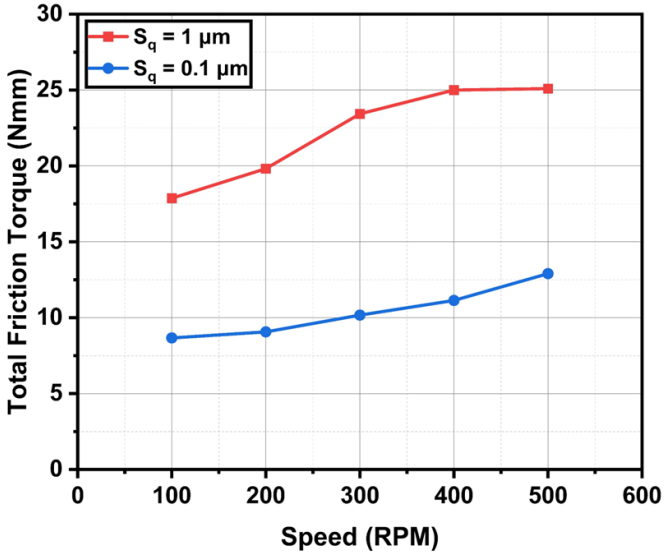

Fig. 6 Plot of change in friction torque

Variation of friction coefficient at the contacts. The effect of surface roughness on friction coefficient (COF) at different locations of contact in a bearing at varying rotational speeds is shown in Fig. 7. In Fig. 7(a), the friction coefficient for the ball-outer race contact decreases with reduced surface roughness, showing higher friction coefficient for the rougher surface as compared to the smoother surface, with minimal impact from speed. Similarly, the friction coefficient at the ball-inner race contact is shown in Fig. 7(b), where a lower coefficient of friction results from a decrease in surface roughness, but speed has minimal bearing on roughness levels. The friction coefficient at the ball-cage contact, on the other hand, is highlighted in Fig. 7(c), where speed and surface roughness both have a substantial impact. At lower speeds, rougher surfaces exhibit higher COF, while smoother surface shows a marked decrease in COF as speed increases, indicating that higher speeds help reduce friction for smoother surfaces in this contact type. Overall, the results indicate that higher surface roughness leads to consistently higher COF values across all contact points and speeds. In contrast, smoother surfaces exhibit a slight reduction in COF with increasing speed, particularly in the ball-cage contact, suggesting reduced frictional losses at higher speeds.

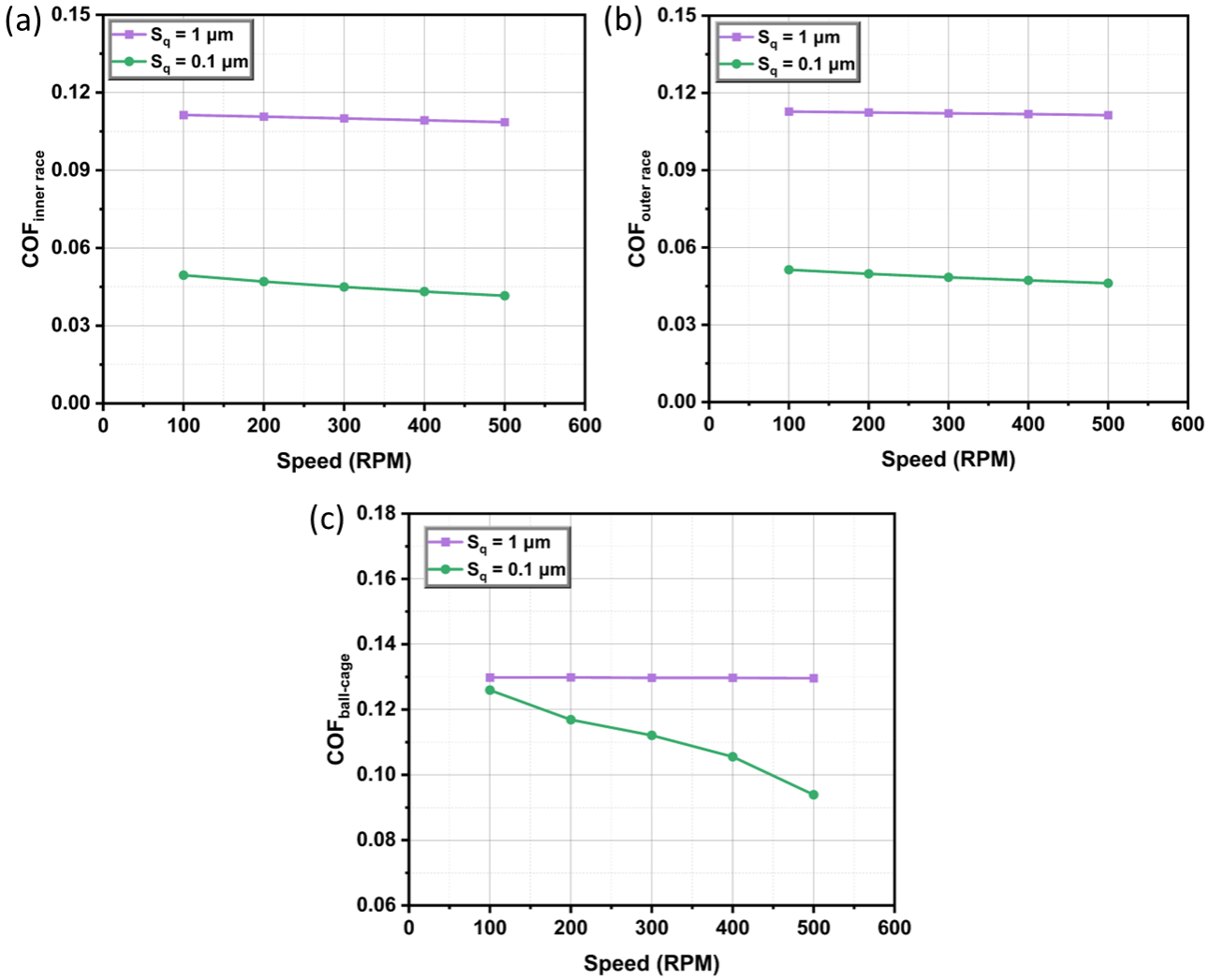

Fig. 7 Coefficient of friction at (a) ball-outer race contact, (b) ball-inner race contact, and (c) ball-cage contact

Variation of friction moment at ball-race and ball-cage contacts. The total friction torque generated in a ball bearing is the sum of friction torque generated at the ball-race interface and the ball-cage interface. Therefore, to understand the effect of speed and surface roughness on the total friction torque, it's necessary to look at how ball-race friction torque and ball-cage friction torque change with these parameters. Fig. 8 comprises three subplots, each analyzing torque as a function of speed for two surface roughness conditions i.e. Sq = 1 µm and Sq = 0.1 µm. From Fig. 8(a), it can be observed that the ball-race torque remains almost constant for Sq = 1 µm, with a value of around 17 Nmm, while for Sq = 0.1 µm, it shows a slight decrease as speed increases, starting at approximately 8 Nmm at 100 RPM and dropping to about 7 Nmm at 500 RPM. Fig. 8(b) shows that the ball-cage friction torque increases with speed. For Sq = 1 µm, the ball-cage torque starts at around 0.6 Nmm at 100 RPM and rises steeply to 8.2 Nmm at 500 RPM. Similarly, for Sq = 0.1 µm, the ball-cage torque grows steadily from about 0.5 Nmm to 6 Nmm over the same speed range, although the values remain lower than those for the rougher surface. Now, Fig. 8(c) depicts the variation of the total friction torque, which is the combined effect of the ball-race and ball-cage torques. For Sq = 1 µm, the total torque increases gradually from 17.89 Nmm at 100 RPM to 25.09 Nmm at 500 RPM. For Sq = 0.1 µm, the total moment starts at around 8.67 Nmm at 100 RPM and increases steadily to approximately 12.90 Nmm at 500 RPM. Overall, the figure highlights the significant influence of surface roughness on torque. Bearings with higher surface roughness (Sq = 1 µm) exhibit consistently higher torque values across all speed ranges. Additionally, the ball-cage torque contributes more

significantly to the total torque at higher speeds, especially for rougher surfaces for the specified range of speeds.

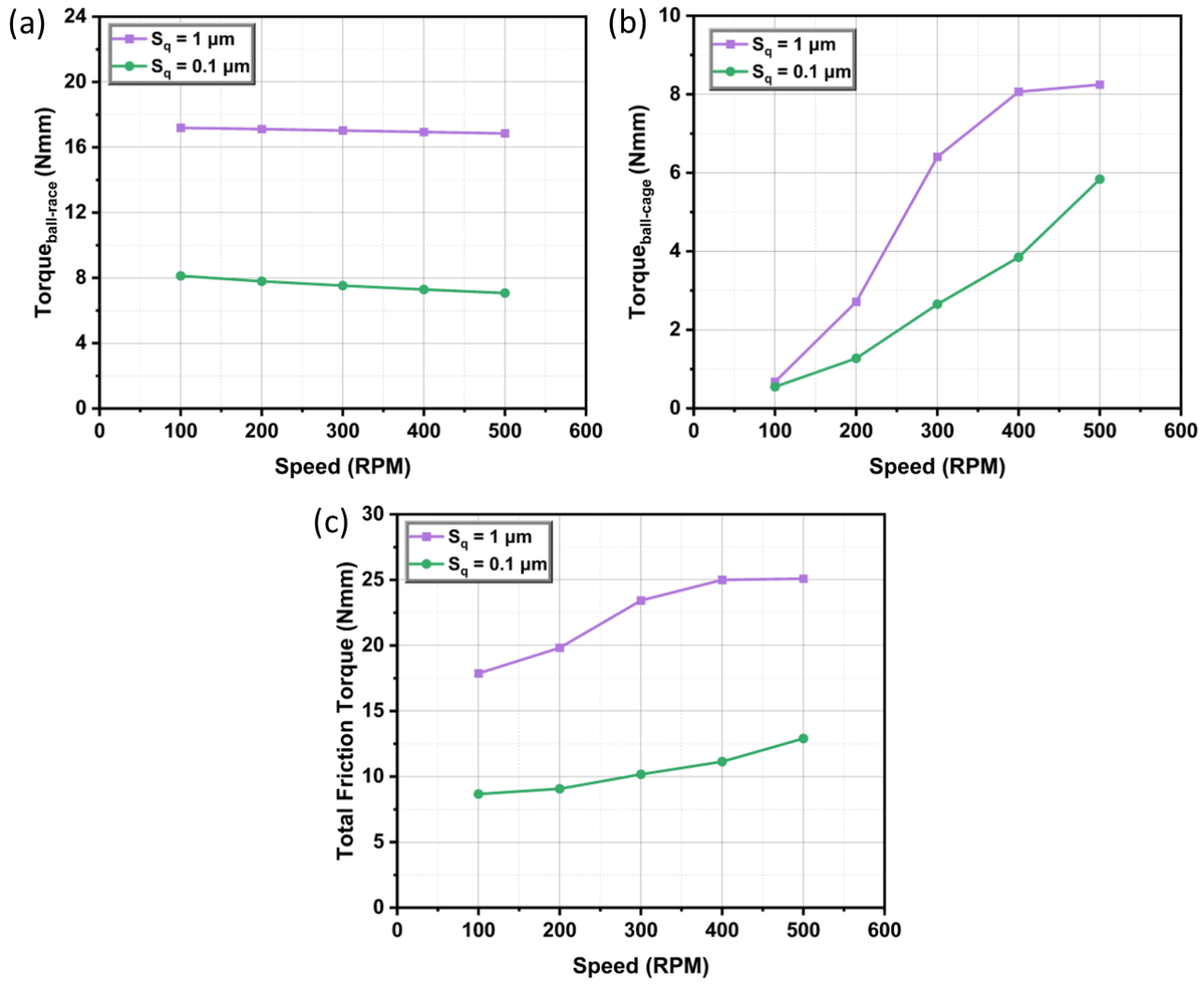

Fig. 8 Friction moment at (a) ball-race contact, (b) ball-cage contact, and (c) ball bearing

Variation of ball-cage contact force. Fig. 9 depicts the relationship between rotational speed and the maximum contact force between ball and cage for surface roughness of Sq = 1 µm and Sq = 0.1 µm. The force is observed to increase as the rotational speed rises, regardless of the surface roughness. For the rougher surface (Sq = 1 µm), the maximum force is consistently higher than for the smoother surface (Sq = 0.1 µm) at all speeds. At 100 RPM, the forces are relatively low, measuring 2.71 N for Sq = 1 µm and 2.08 N for Sq = 0.1 µm. As the speed increases to 500 RPM, the forces rise significantly to 27.95 N and 12.88 N for Sq = 1 µm and Sq = 0.1 µm, respectively. This pattern is evident at all speeds, demonstrating that both increased speeds and surface roughness contribute to increased contact forces. Because friction moment is directly influenced by contact force, the higher contact force results in an increase in friction moment at the ball-cage contact.

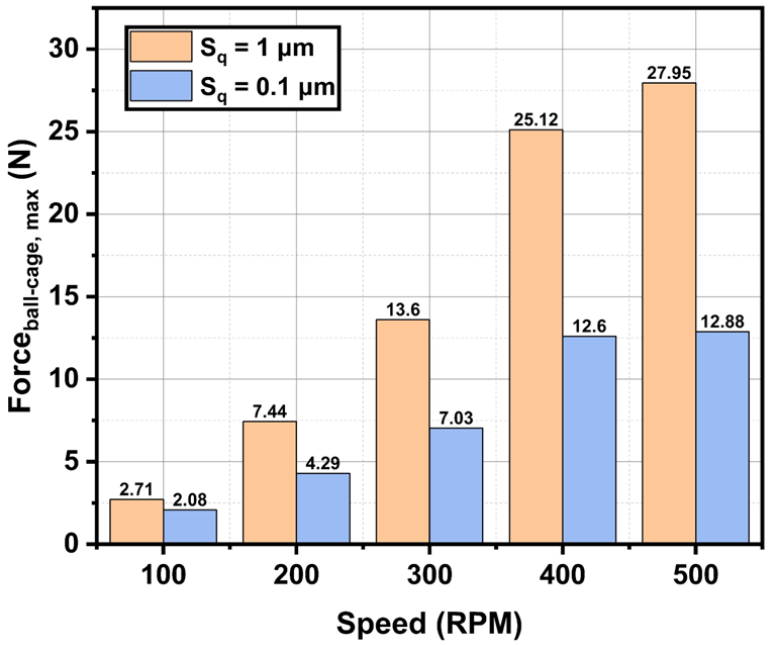

Fig. 9 Change in ball-cage contact force

Summary

The presented analysis highlights the significant effect of surface roughness and speed on the friction torque of a 6205 ball bearing. Bearings with higher surface roughness (Sq = 1 µm) consistently exhibit greater friction torque than those with smoother surfaces (Sq = 0.1 µm) across all speeds. Friction moment increases with rotational speed for both surface roughness, with rougher surfaces amplifying frictional losses more significantly. The ball-cage contact contributes substantially to total torque at higher speeds, especially for rougher surfaces, due to the increased contact forces. These findings emphasize the importance of smoother surfaces in minimizing friction torque and reducing frictional losses, particularly at higher rotational speeds.

References

[1] C. Jin, B. Wu, Y. Hu, Heat generation modeling of ball bearing based on internal load distribution, Tribol. Int. 45 (2012) 8-15.

[2] R.D. Mindlin, Compliance of elastic bodies in contact, J. Appl. Mech. (1949) 259-268.

[3] M.J. Todd, K.L. Johnson, A model for coulomb torque hysteresis in ball bearings, Int. J. Mech. Sci. 29 (1987) 339-354.

[4] S. Jiang, X. Chen, J. Gu, X. Shen, Friction moment analysis of space gyroscope bearing with ribbon cage under ultra-low oscillatory motion, Chin. J. Aeronaut. 27 (2014) 1301-1311.

[5] C.G. Zhou, L.D. Wang, J.W. Shen, C.H. Chen, Y. Ou, H.T. Feng, Wear characterization of raceway surface profiles of ball screws, J. Tribol. 144 (2022) 111701.

[6] B. Bachchhav, H. Bagchi, Effect of surface roughness on friction and lubrication regimes, Mater. Today Proc. 38 (2021) 169–173.

[7] X. Li, Y. Liu, J. Huang, D. Sang, K. Yang, J. Ling, Influence of surface texture on pocket pairs lubrication performance of cylindrical roller bearings, Ind. Lubr. Tribol. 76 (2024) 1085–1097.

[8] B. Gouda, N. Tandon, R.K. Pandey, C.K. Babu, Effects of positioning of inner race micro-textures on the tribodynamic performances of radial ball bearings, Mech. Syst. Signal Process 223 (2025) 111908.

[9] C.F. Han, H.Y. Chu, R.Y. Luo, N.T. Liao, C.C. Wei, G.L. Chen, Effects of groove factor and surface roughness of raceway in ball-bearing-like specimens on tribological behavior and the onsets of two instabilities of dry contacts, Wear 406 (2018) 126–139.

[10] H. Kumar, V. Gupta, V. Bharath, M. Tiwari, S.K. Paul, L. Agrawal, A.P. Singh, A. Jain, Effect of Surface Roughness on the Friction Moment in a Lubricated Deep Groove Ball Bearing, Lubricant 12 (2024) 443.

[11] K.L. Johnson, Contact mechanics, Cambridge University Press, UK, 1987.

[12] K.L. Johnson, J.A. Greenwood, S.Y. Poon, A simple theory of asperity contact in elastohydrodynamic lubrication, Wear 19 (1972) 91–108.

[13] Y. Zhao, D.M. Maietta, L. Chang, An asperity microcontact model incorporating the transition from elastic deformation to fully plastic flow, J. Trib. 122 (2000) 86–93.

[14] G. Nijenbanning, C.H. Venner, H. Moes, Film thickness in elastohydrodynamically lubricated elliptic contacts, Wear 176 (1994) 217–229.